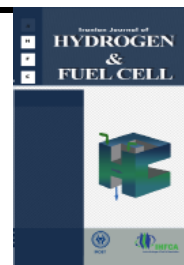


Iranian Journal of Hydrogen & Fuel Cell

IJHFC

Journal homepage://ijhfc.irost.ir



The effect of increasing the multiplicity of flow fields contact surface on the performance of PEM fuel cell

Farzin Ramin¹, Sima Baheri Islami^{1,*}, Siamak Hossainpour²

¹Faculty of Mechanical Engineering, University of Tabriz, Tabriz, Iran

²Mechanical Engineering Faculty, Sahand University of Technology, Tabriz, Iran

Article Information

Article History:

Received:

17 Apr 2017

Received in revised form:

14 Aug 2017

Accepted:

16 Aug 2017

Keywords

Solid oxide fuel cells
PEM Fuel cell
Power density
Reactive area
Electrochemical reaction

Abstract

In this paper, three innovative 3-D geometries for flow fields of cathode and anode have been developed to investigate the comparative impact of increasing the multiplicity of the involved anode-cathode channel surface contact on the efficiency of electrochemical reaction via the same membrane electrode assembly (MEA) active area. In the introduced new models, each anode channel includes two, three and four cathodes while the convectional model include a one to one connection. The governing equations consist of mass, momentum and energy conservation. In addition, the species transport and the electric/ionic fields were solved numerically using the finite volume method under the assumptions of steady state and non-isothermal fluid flow. Simulation results revealed that increasing the multiplicity of the anode-cathode involved surface of reactants channel leads to current and power density enhancement due to the improved opportunity of reactants penetration and less concentration losses. Also, a considerable reduction of mono-cell volume size and costs for the new models in comparison with the base design was achieved.

1. Introduction

Polymer electrolyte membrane (PEM) fuel cells are widely accepted as the upcoming generation of

Polymer electrolyte membrane (PEM) fuel cells are widely accepted as the upcoming generation of power sources due to their reliable efficiency in the conversion of hydrogen reactant, as the inlet fuel,

*Corresponding Author's Fax: +98-041-33354153

E-mail address: baheri@tabrizu.ac.ir

and air or pure oxygen, as the oxidant, to electrical energy output. Moreover, their lower production rate of pollutants and greenhouse gases during the electrochemical reaction and flexibility of utilization for minor and major energy production fields are some of the potential advantages of this type of fuel cells. PEM fuel cells face some obstacles in their commercial mass production in which expense of fabrication and efficiency of their performance are important factors. Innovative changes in the geometry and construction of the PEM fuel cell have improved their performance while simultaneously decreasing fabrication costs [1-5]. Traditional geometry of the PEM fuel cell consists of a polymer membrane impregnated by catalyst layers surrounded by gas diffusion layers and reactants channels and bipolar plate for both anode and cathode sides. The architecture of bipolar plates and the determination of channel configuration is an important factor for increasing the current density in PEM fuel cells. While plenty of research has been done to overcome geometrical challenges [6-9], some of these difficulties remain unresolved [10, 11]. The geometry scheme of reactants flow field and the design of supplying and distributing reactants inside the cell play remarkable roles in the efficiency, durability and cost of a PEM fuel cell [12-14]. The non-uniformity of species distribution, membrane drying or flooding, lack of enough reactants diffusion and low output current density are some of challenges conventional PEM fuel cell design face. In recent years researchers have tried to present innovative designs to remove these issues instead of working on increasing the performance and reducing the volume and construction costs of the PEM fuel cell. Ghanbarian et al. [15] studied the influence of flow channel indentation on the performance of a PEM fuel cell. They showed that the performance of the cell was enhanced by partial blockage of the flow channels in a parallel flow field because the channel indentation could increase oxygen content within the catalyst layer. It was observed that the influence of implementing indentation to the channels in high current density regions was noticeable. Seven novel

gas flow fields of a PEM fuel cell were analyzed by Rahimi-Esbo et al. [16] and the cells performance was investigated at the optimum channel to rib ratio. The results showed that a 2-1-serpentine flow field has the highest performance especially at high current densities. It was found that for operating voltages over 0.5 V, the geometry of the flow channels does not have a significant effect on performance; moreover, the local stoichiometry at the terminal region increased using this new flow field, leading to lower possibility of flooding and slug flow in this area. Vazifeshenas et al. [17] presented a novel compound gas flow field geometry along with typical serpentine and parallel designs which were verified through 3-D simulations. Comparison of the polarization curve of the novel compound design along with other contours indicated that it could be a viable choice for flooding phenomena prevention, while its performance was approximately the same as the serpentine type. Torkavannejad et al. [18] presented a complete three-dimensional and single phase model for an innovative design of a PEM fuel cell to investigate the effect of using different channel and reactant supply on the performances, current density, and temperature and gas concentration distributions. They concluded that the performance of the cell increased in these novel designs, which performed extra connections of channels, and the occupied volume and cost decreased by using these geometries. Rostami et al. [19] studied the serpentine gas flow channel with different bend sizes of a PEM fuel cell. The results revealed that increments in the bend size of 0.2 mm lead to a decrease in over potential as well as the temperature gradient. By uniform distribution of electrolytes over the electrode area, the power density of the cell increased 1.78% in comparison with conventional geometry. Pourmahmoud et al. [20-22] developed different channel geometries in order to enhance PEM fuel cell's performance. The research indicated that an elliptical and circular channel cross-section had the potential to produce higher current density in comparison with conventional PEM fuel cells. Moreover, the

elliptical and circular channel designs enhanced the reactant transportation, led to more uniform distribution of reactants and effectively decreased the loss of mass transport. These factors decreased cathode overpotential which is the main cause of loss in PEM fuel cells. Investigating the gas flow channel with obstacles in different operating conditions of temperature, stoichiometry and relative humidity was done by Bilgili et al. [23]. Results indicated that the new geometry lead to reactants concentration distribution along the flow field as well as diffusion of species to the gas diffusion layer, and as a result the power and current density increased. Ramin et al. [24] investigated the effect of an inclined radial gas flow channel in the radial stack of a PEM fuel cell. Comparison of polarization curves indicated that the cell with an inclined radial channel produced more current density at the same reaction and inlet area, which make it a strong candidate for future PEM fuel cell geometry design. A numerical model was introduced by F. Tiss et al. [25] to study mass transport in a cell with geometry of partial blocks inserted in the gas channel to guide the reactants for better diffusion into the gas diffusion layer. The final results indicated that partial blocks in the gas flow field lead to enhancement of performance. Khazaei et al. [26] presented a series of new geometry by investigating the different scenarios of connecting the bipolar plate to the gas diffusion layer of a PEM fuel cell. The current and power density curves revealed that increasing connections between the bipolar plate and gas diffusion layer improves the performance of the cell.

Based on previous studies, it can be concluded that an efficient geometry design of a PEM mono-cell leads to the enhancement of the cell performance. In this research, a comparative study was performed to investigate the effect of increasing the number of reactants channels in connection with each other. Four cases include one anode channel with one, two, three and four cathode channels were investigated. Increment of channels contact surface with each other provides more opportunity for reactants to diffuse into the reaction layer. As a result, the enhancement

of reaction rate leads to the improvement of output current density. Simulation of the mentioned models were performed by a three-dimensional, single phase and non-isothermal computational fluid dynamics analysis. The introduced layouts were also simulated by the identical flow feed compositions, flow rates and the same anode and cathode side's boundary conditions. The current study presents a comprehensive comparison between the new designs and a base model in terms of current and power density, reactant consumption, and so on.

2. System description

Schematic of the mono-cells and stack ordering for the base model (case one) and the three new designs (case two, three and four) presented for the PEM fuel cell are indicated in Fig. 1. In these geometries, each anode channel is in contact with one, two, three and four cathode channels, respectively. (A) and (C) stand for anode and cathode channels, respectively. In all designs, the active reaction area of membrane electrode assembly is the same value to allow for comparison. This novel feature provide more accessibility of reactants to reaction layer, and therefore has the capability of enhancing current density. The geometric and operational parameters of these designs are shown in Tables 1 and 2 [18]. Fig. 1 also indicates the traditional domain of the conventional PEM fuel cell and the same MEA layer specifications for all the cases. In this regard, all the boundary conditions, the active area and the inlet flow specifications are the same for all cases. All considered cases of the PEM fuel cell consist of fuel and oxidant channels and bipolar plates on both cathode and anode sides. The MEA consist of gas diffusion and catalyst layers sandwiched between the gas flow field channels. The third and fourth cases support the promising new stacks introduced, especially in terms of proper reactant distribution and methods of reactants supply, smaller used volume, less bipolar plates required, and the potential for enhancing the PEMFC performance.

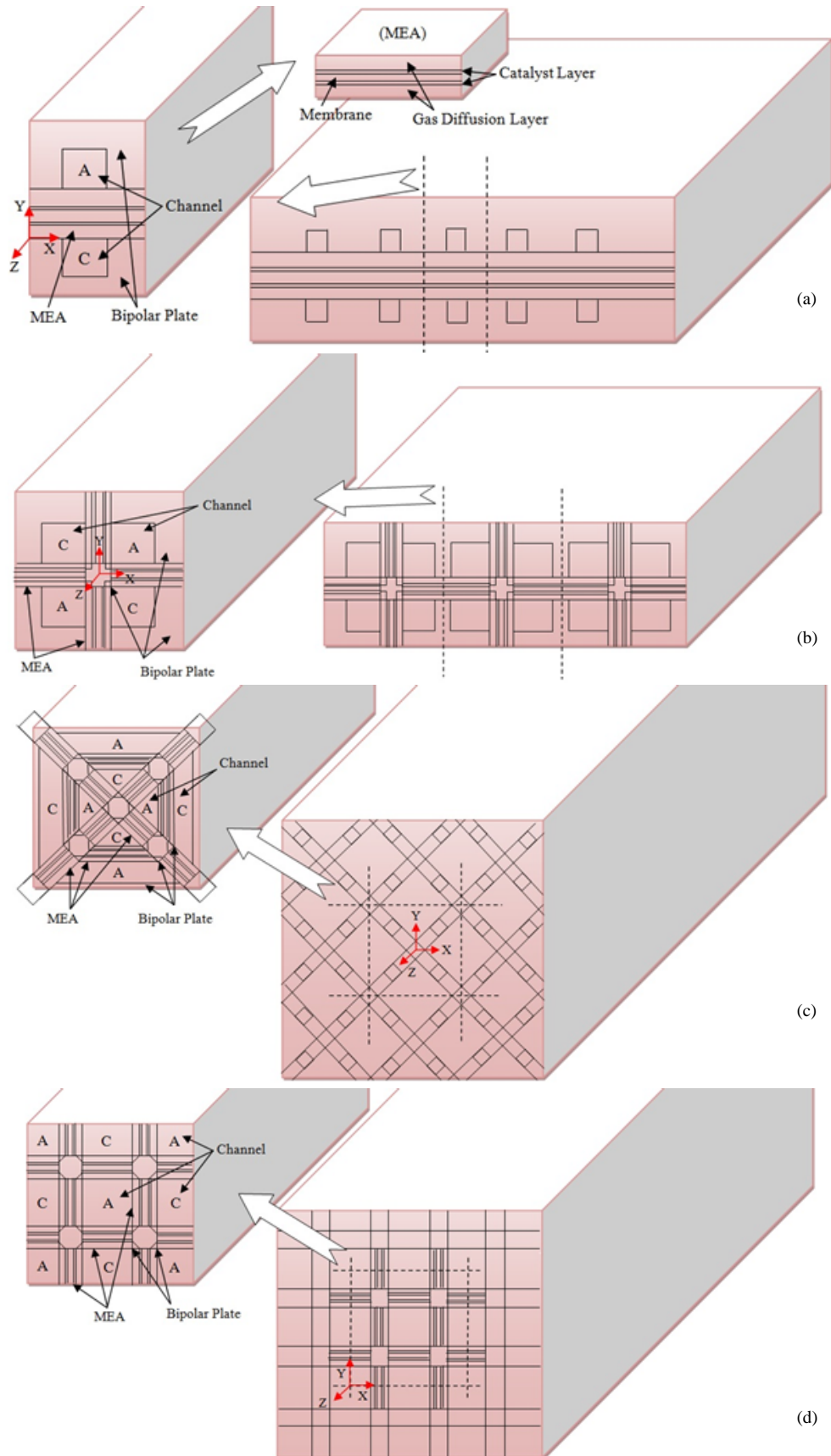


Fig. 1. Schematic of the stack and mono-cell computational domain for a) case one, b) case two, c) case three and d) case four

Table 1. Geometric parameters of conventional architecture (case one) and three new designs (case two, three and four)

Parameter	Units	Case one	Case two	Case three	Case four
Active cell area	m ²	1.0e ⁻⁴	1.0e ⁻⁴	1.0e ⁻⁴	1.0e ⁻⁴
Channel width (W)	m	1.0e ⁻³	0.7e ⁻³	1.42e ⁻³ /4.25e ⁻³ (base of the triangles)	1.0e ⁻³
Shoulder thickness (d _s)	m	0.5e ⁻³	0.3e ⁻³	0.23e ⁻³	0.26e ⁻³
Cell length (L)	m	0.5e ⁻¹	2.5e ⁻²	7.33e ⁻³	12.5e ⁻³
Bipolar plate required	m ³	2.0e ⁻⁷	57.76e ⁻⁹	33.55e ⁻⁹	6.76e ⁻⁹
Gas diffusion layer thickness (δ _{GDL})	m	0.26e ⁻³	0.26e ⁻³	0.26e ⁻³	0.26e ⁻³
Wet membrane thickness (Nafion 117)	m	0.23e ⁻³	0.23e ⁻³	0.23e ⁻³	0.23e ⁻³
Catalyst layer thickness (δ _{CL})	m	0.287e ⁻⁴	0.287e ⁻⁴	0.287e ⁻⁴	0.287e ⁻⁴
GDL porosity (ε)	-	0.4	0.4	0.4	0.4
CL porosity (ε)	-	0.4	0.4	0.4	0.4

Table 2. Geometric parameters, component specifications and operating conditions for the conventional PEMFC as a base design

Parameters	Symbol	Value	Unit
Channel length	L	0.5 e ⁻¹	m
Channel width	W	1 e ⁻³	m
Channel height	H	0.1 e ⁻³	m
Shoulder thickness	d _s	0.5 e ⁻³	m
Anode pressure	P _a	3	atm
Cathode pressure	P _c	3	atm
Inlet fuel and air temperature	T _{Cell}	353.15	K
Thermal conductivity	k	0.15	W/K.m
Relative humidity of inlet fuel and air (fully humidified conditions)	ψ	100	%
Reference current density	I	10	A/cm ²
Inlet anode oxygen mass fraction	Y _{OXYGEN,A}	0	-
Inlet anode hydrogen mass fraction	Y _{HYDROGEN,A}	0.3780066	-
Inlet anode water mass fraction	Y _{WATER,A}	0.6219934	-
Inlet cathode water mass fraction	Y _{WATER,C}	0.1031307	-
Inlet cathode oxygen mass fraction	Y _{OXYGEN,C}	0.2088548	-
Inlet cathode hydrogen mass fraction	Y _{HYDROGEN,C}	0	-
Faraday constant	F	96.487	C/mol
H ₂ diffusivity	D _{H2}	1.1e ⁻⁴	m ² /s
O ₂ diffusivity	D _{O2}	3.23e ⁻⁵	m ² /s
H ₂ O diffusivity at anode	D _{H2O;a}	7.35e ⁻⁵	m ² /s
H ₂ O diffusivity at cathode	D _{H2O;c}	7.35e ⁻⁵	m ² /s
Anode transfer coefficient	α _a	0.5	-
Cathode transfer coefficient	α _c	2	-

3. Multi-dimensional non-isothermal model

3.1. Model assumptions

The presented designs consider the electrochemical kinetics, current and temperature distributions, flow fields over the bipolar plates and multi-component

transport of oxidizer (air) and fuel (Hydrogen) streams in a three-dimensional domain. The model assumptions include:

- (I) steady state condition and non-isothermal design;
- (II) ideal gas mixtures behavior;
- (III) homogeneous and isotropic porous mediums of gas diffusion layers and catalyst layers;
- (IV) laminar and incompressible

flow due to the low pressure gradients and flow velocities; (V) fully humidified membrane to transport the protons and impermeable to cross-over of reactant gases over the membrane; (VI) fully humidified reactants condition for both anode and cathode inlets; (VII) single phase simulation (the volume of liquid-phase water produced during the reactions is neglected and phase change or two-phase transports are not considered); (VIII) negligible Ohmic resistance at porous electrodes and current collectors; (IX) the dilute solution theory (considered for the species diffusion); and (X) Butler-Volmer kinetic equation (used for the electrochemical reactions at the electrodes). All governing equations [18] were solved under the following boundary condition for the simulation of electrochemical phenomena at the different areas of the cell including the membrane, gas flow fields, gas diffusion layers and catalyst layers layer, and are listed in Table 3.

3.2. Boundary conditions

The velocities at the cathode and anode channel inlets are calculated based on the stoichiometries. Constant mass flow rate is considered at the channel inlet and pressure is set to zero at the channel outlet since the outlet stream discharges to the atmosphere. Zero gradients at the channel outlets are considered for other variables.

No mass flux condition is considered at all walls and symmetry conditions at the side faces are applied. Total mass fractions of reactants are equal in channels inlets.

According to the ideal gas law, the inlet mass fractions are determined by the inlet pressure and humidity. The equations for both anode and cathode sides are expressed as Eq. (23), where the parameter i_{avg} is the average current density at a given cell potential. R , T_{in} , P_{in} , and ξ are the universal gas constant, inlet temperature, inlet pressure and the stoichiometric ratio, respectively.

The stoichiometric ratio is defined as the ratio between the amount of supplied and the amount of

required reactant on the basis of the reference current density i_{avg} , accordingly. The other inlet conditions are shown in Table 2.

4. Numerical implementation

The computational fluid dynamics software, Fluent, was used by exerting the SIMPLE pressure-velocity coupling algorithm to solve the model governing equations. The model's mesh was investigated for the grid size independency of the solutions. The computational domain was divided into approximately 176000 unstructured cells according to the number of iterations and accuracy regards. About 3500 iterations were performed and the convergence criterion between accurate iterations was less than 10^{-7} for all parameters. The estimated computational running time was about eight hours.

5. Results

5.1. Validation of numerical model

The variation of the cell potential versus current density for the conventional base cell has been compared with the experimental results of Al-Baghdadi et al. [27]. Fig. 2 indicates this comparison along with an example of grid independency test which reveals that 176000 cells in the computational domain is an acceptable selection. Fig. 3 also reveals some deviations from experimental results especially at high current densities. This can be due to the phase change in experimental cases which has been neglected in the numerical simulation. In the experimental model, the produced liquid phase water blocks the porous medium of the catalyst and gas diffusion layers which prevent the reactants crossing and leads to performance loss. The output cell current and power density are the common criteria for the evaluation of PEM fuel cell efficiency. Variation of current and power density with the cell voltage are shown in Figs. 4 and 5. Power density is

Table 3. Governing equations [18]

Eq.	Equation	Equation name	Parameter/ Variable
(1)	$\nabla \cdot (\rho u) = 0$	Continuity equation	Gas flow field
(2)	$\nabla \cdot (\rho u u - \mu \nabla u) = -\nabla \left(P + \frac{2}{3} \mu \nabla u \right) + \nabla \cdot [\mu (\nabla u)^T]$	Momentum equations	Gas flow field
(3)	$\nabla \cdot [-\rho y_i \sum_{j=1}^N D_{ij} \frac{M}{M_j} (\nabla y_i + y_i \frac{\nabla M}{M})] + \rho y_i u = 0$	Mass transport equation for species i	Mass balance and species concentration
(4)	$D_{ij} = \frac{T^{1.75} \times 10^{-3}}{P \left[\sum_k V_{ki} \right]^{1/3} + \left(\sum_k V_{kj} \right)^{1/3}} \left[\frac{1}{M_i} + \frac{1}{M_j} \right]^{1/2}$	Kinetic gas theory	Maxwell-Stefan diffusion coefficients
(5)	$\nabla \cdot (\rho C_p u T - k \nabla T) = 0$	Energy equation	Temperature
(6)	$\nabla \cdot (\rho \varepsilon u) = 0$	Continuity equation in gas diffusion layers	Transport in gas diffusion layers
(7)	$u = \frac{K_p}{\mu} \nabla P$	Darcy's law	Momentum equation in gas diffusion layers
(8)	$\nabla \cdot [-\rho \varepsilon y_i \sum_{j=1}^N D_{ij} \frac{M}{M_j} (\nabla y_i + y_i \frac{\nabla M}{M})] + \rho \varepsilon y_i u = 0$	Continuity equation in porous media	Mass transport equation in porous media
(9)	$D_{ij}^{eff} = D_{ij} \times \varepsilon^{1.5}$	Bruggemann correction formula	Diffusivity in porous media
(10)	$\nabla \cdot (\rho \varepsilon C_p u T - k_{eff} \varepsilon \nabla T) = \varepsilon \beta (T_{solid} - T)$	Energy equation for the gas diffusion layers	Heat transfer in gas diffusion layers
(11)	$\nabla \cdot (\sigma_{GDL} \nabla \phi) = 0$	Potential equation for the gas diffusion layers	Potential distribution in gas diffusion layers
(12)	$S_{O_2} = -\frac{M_{O_2}}{4F} i_c$	Sink term for oxygen	Oxygen consumption
(13)	$S_{H_2} = -\frac{M_{H_2}}{4F} i_a$	Sink term for hydrogen	Hydrogen consumption
(14)	$S_{H_2O} = -\frac{M_{H_2O}}{2F} i_c$	Source term for water	Water production
(15)	$\dot{q} = \frac{T(-\Delta S)}{n_e F} + \eta_{act,c} i_c$	Heat generation equation	Heat generation in the cell
(16)	$i_c = i_{O_2,C}^{ref} \left(\frac{C_{O_2}}{C_{O_2}^{ref}} \right) \left[\exp \left(\frac{\alpha_a F}{RT} \eta_{act,c} \right) + \exp \left(-\frac{\alpha_c F}{RT} \eta_{act,c} \right) \right]$	Butler-Volmer equation (cathode)	Cathode current density & overpotential
(17)	$i_c = i_{O_2,a}^{ref} \left(\frac{C_{H_2}}{C_{H_2}^{ref}} \right) \left[\exp \left(\frac{\alpha_a F}{RT} \eta_{act,a} \right) + \exp \left(-\frac{\alpha_a F}{RT} \eta_{act,a} \right) \right]$	Butler-Volmer equation (anode)	Anode current density & overpotential
(18)	$\eta_{act} = E - E_{eq}$	Activation potential	Electrode potential
(19)	$N_w = n_d M_{H_2O} \frac{i}{F} - \nabla \cdot (\rho D_w \nabla y_w)$	Water balance for the membrane	Net water flux through the membrane
(20)	$n_d = 2.5 \lambda / 22$	Electro-osmotic drag coefficient	Membrane water content
(21)	$\nabla \cdot (k_{Mem} \nabla T) = 0$	Energy balance for the membrane	Heat transfer in the membrane
(22)	$\nabla \cdot (\sigma_{Mem} \nabla \phi) = 0$	Potential equation for the membrane	Potential loss across the membrane
(23)	$ \vec{u} _{in} = \frac{\zeta}{X_{H_2,in}} \frac{I_{avg}}{2F} \frac{RT_{in}}{P_{in}} \frac{A_{MEA}}{A_{ch}}$	Inlet velocity (boundary condition)	Average current density

calculated by multiplying the current density at the cell related voltage. Results reveal that increasing the connection of flow fields by the next cases leads to performance improvement; specifically at medium to high current densities ranges, which are the customary period of operating condition in PEM fuel cells. The fourth case, the connection of each anode channel to four cathode ones, expresses the best performance among the considered cases.

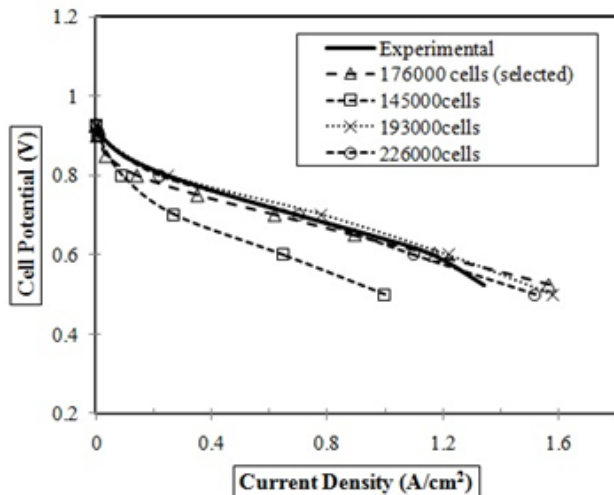


Fig. 2. The variation of cell potential versus current density for current data and experimental results of Al-Baghdadi et al. [27].

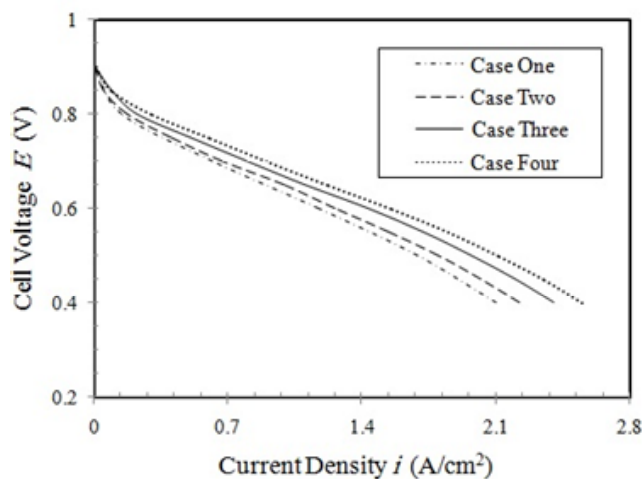


Fig. 3. Variation of cell potential versus current density for the studied cases.

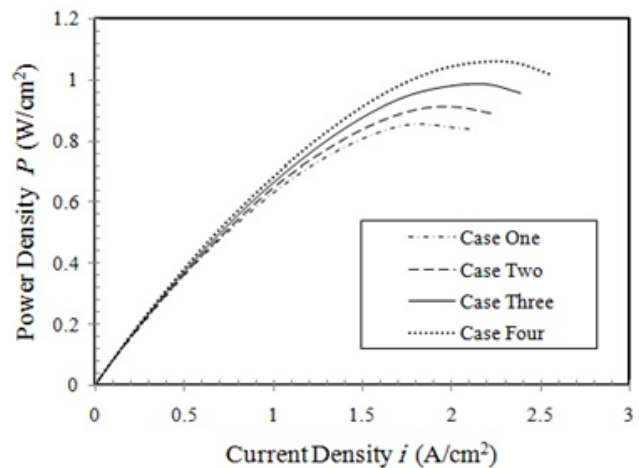


Fig. 4. Variation of cell power density versus current density for the studied cases.

5.2. Comparison of size and cost aspects of the new designs

Table 1 presents comprehensive and comparative data on the geometrical characteristics of the three new cases and the base model of the PEM fuel cell. The active reaction area of membrane electrode assembly is a fixed value for all cases (100 mm^2). Conversely, results show that the mono-cell volume of case two (197.03 mm^3) and case four (163.33 mm^3) are smaller than the base case (380.74 mm^3). The volume of the bipolar plates in the base case (200 mm^3) is sensibly larger than case two (57.76 mm^3), three (50.61 mm^3) and four (46.76 mm^3). Based on the fixed active reaction area which leads to the same volume of the membrane electrode assembly, cases two and three require less volume for the bipolar plate up to. This fact leads to a lower final cost for the stack due to the high price of bipolar plates [28, 29]; hence, the new architectures are more beneficial than conventional designs.

5.3. Distribution of oxygen over the cathode catalyst layers

The oxygen consumption at the cathode catalyst layer as the oxidant plays an important role in the electrochemical reaction rate, which affects the cell efficiency. Fig. 5 illustrates the gradual and uniform

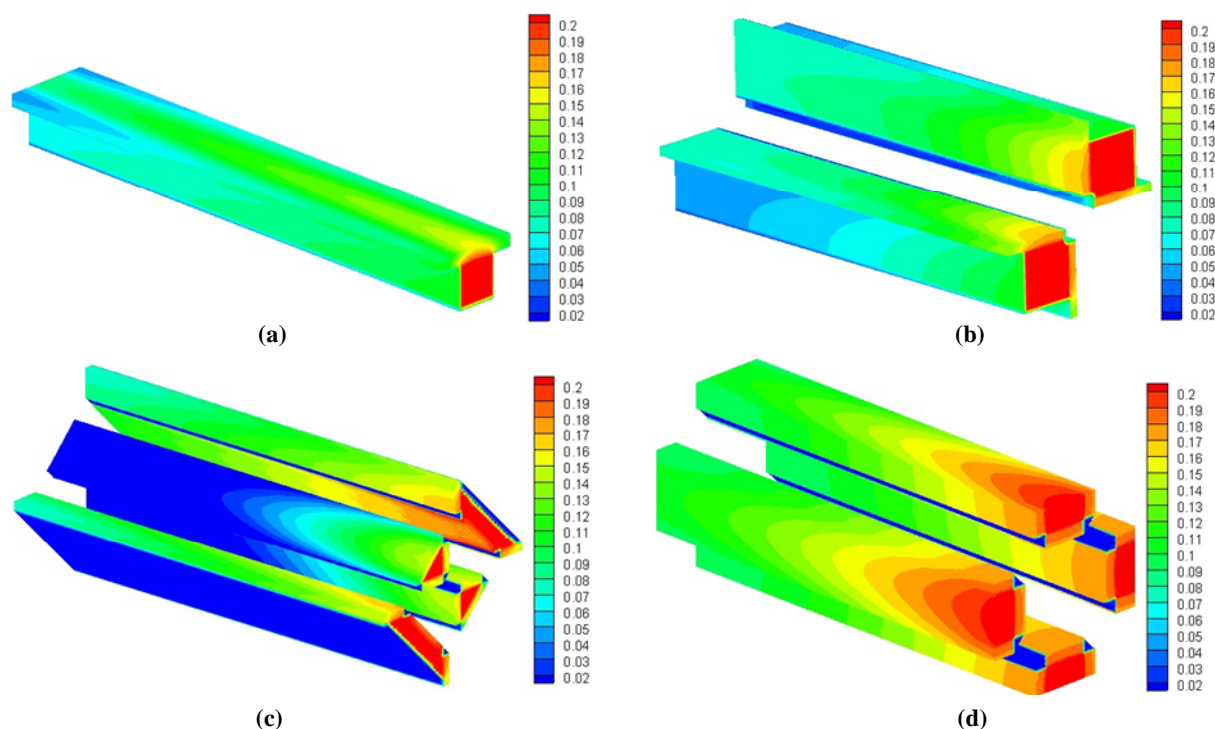


Fig. 5. The distribution of the Oxygen mass fraction along the cathode electrode of the cell for a) case one, b) case two, c) case three, and d) case four at the 0.4 V of cell potential.

decrement of oxygen mass fraction from inlet diffused active area to the outlet for both the new cases and conventional design over the cathode catalyst layer at a potential of 0.4 V. The contour comparison indicates that the new architectures have less dead zone area of diffusion and more uniform distribution of oxygen simultaneously (except the triangular flow channels in the third case because of strong oxygen consumption) which leads to the improvement of produced output current density.

5.4. Distribution of water vapor over the cathode catalyst layers

Management of water species in the cathode catalyst layer is one of the determining factors in the review of cell function. The gas phase water mass fraction at the interface of membrane and cathode catalyst layer of 0.4 V cell potential is shown in Fig. 6 for all cases. The water presence at the cathode catalyst layer is due to three important factors:

(I) the humidity along with the inlet species of cathode

side, (II) the net water transport via the proton ions crossing the membrane from the anode electrode to cathode side as a result of electro-osmotic effect, and (III) the water production during the electrochemical reaction. Results indicate considerable uniformity of the water mass fraction for the new configurations in comparison to the conventional model, which is due to the uniform diffusion of reactants throughout activation over the reaction area. Optimal outflow of produced water is one of the major parameters of water management. This outflow is satisfactory in the multiplicity of flow channels in the proposed cases as compared to the base model.

By moving toward the end of the cathode channel, blocking the porous gas diffusion layer by increasing saturated water leads to increasing of cathode over-potential and concentration losses over the catalyst layers, consequently decreasing the output current and uniformities which will result in mechanical stress on the cell threatening the MEA durability.

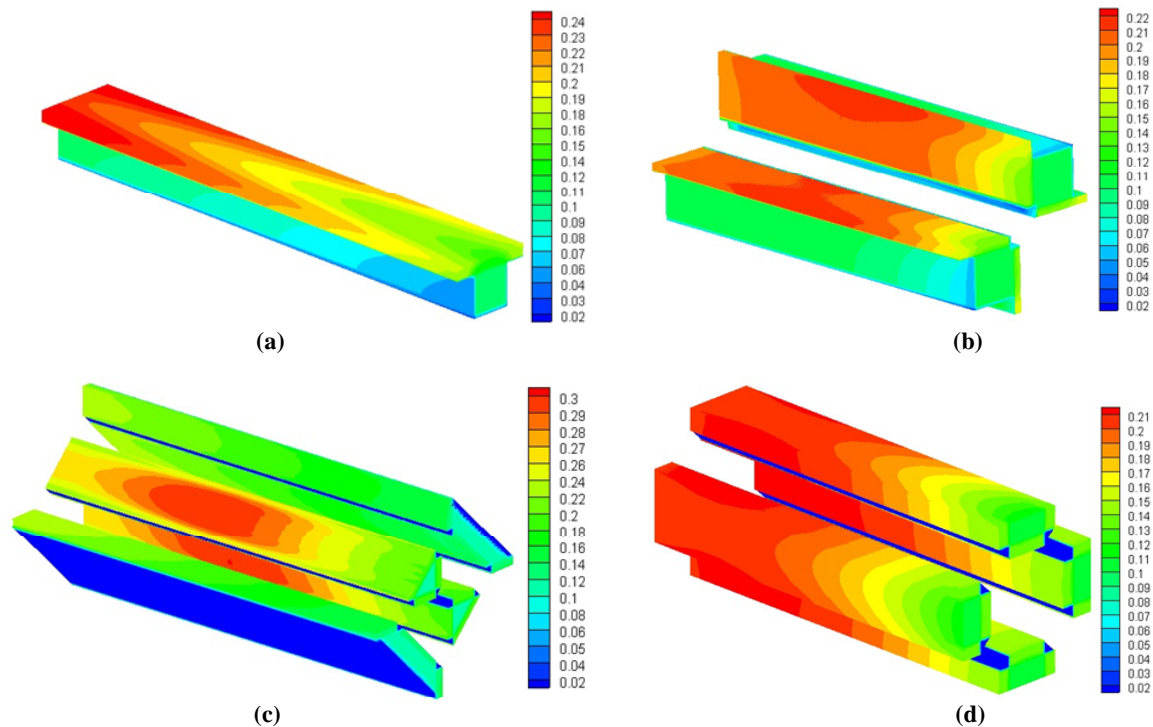


Fig. 6. The distribution of water vapor mass fraction along cathode electrode of the cell for a) case one, b) case two, c) case three, and d) case four at the 0.4 V of cell potential.

5.5. Temperature distribution over the cathode catalyst layer

Temperature distribution within the PEM fuel cell depends significantly on the rate of heat produced by the electrochemical reactions. Due to the exothermic electrochemical reaction, the maximum thermal zone occurs at the interface of the membrane and cathode catalyst layer, as presented in Fig. 7, for the cell voltage of 0.4 V. It can be observed that away from the bipolar plates the temperature is going to rise due to the lack of conductive heat transfer through the shoulders which also increases the traversed distance of gases on the surface, leading to a decrease the temperature at the stagnation area of temperature contours.

As it is shown in Fig. 6, the water vapor concentration increases along the flow field which leads to the temperature adjustment until the outlet region based on the results of Fig. 7. The increment in the temperature leads to an increment in the ionic conduction coefficient and accordingly an increase in the proton crossing over the membrane

rate which finally leads to the sensible increment of output current density. By increasing the effective flow field contact area, the temperature gradient decreases due to the uniformity of distribution. Due to the low membrane thermal conductivity and unrecognizable heat production of anode side, the temperature distribution is almost homogenous and equivalent to the entranced fuel temperature.

5.6. Distribution of current density magnitude

The current density magnitude distribution is displayed for the new designs and the conventional model at the cell potential of 0.4 V over the cathode catalyst layer in Fig. 8. From the inlet to outlet area, the current flux density decreases due to the decrement of reactants concentration through the flow pass over and also an increase of water saturation in the gas diffusion layers. The maximum concentration of current density happens at the intersection of the gas diffusion layers and bipolar plates. Multiplicity of the bipolar plates connected to the membrane electrode assembly and also the number of flow

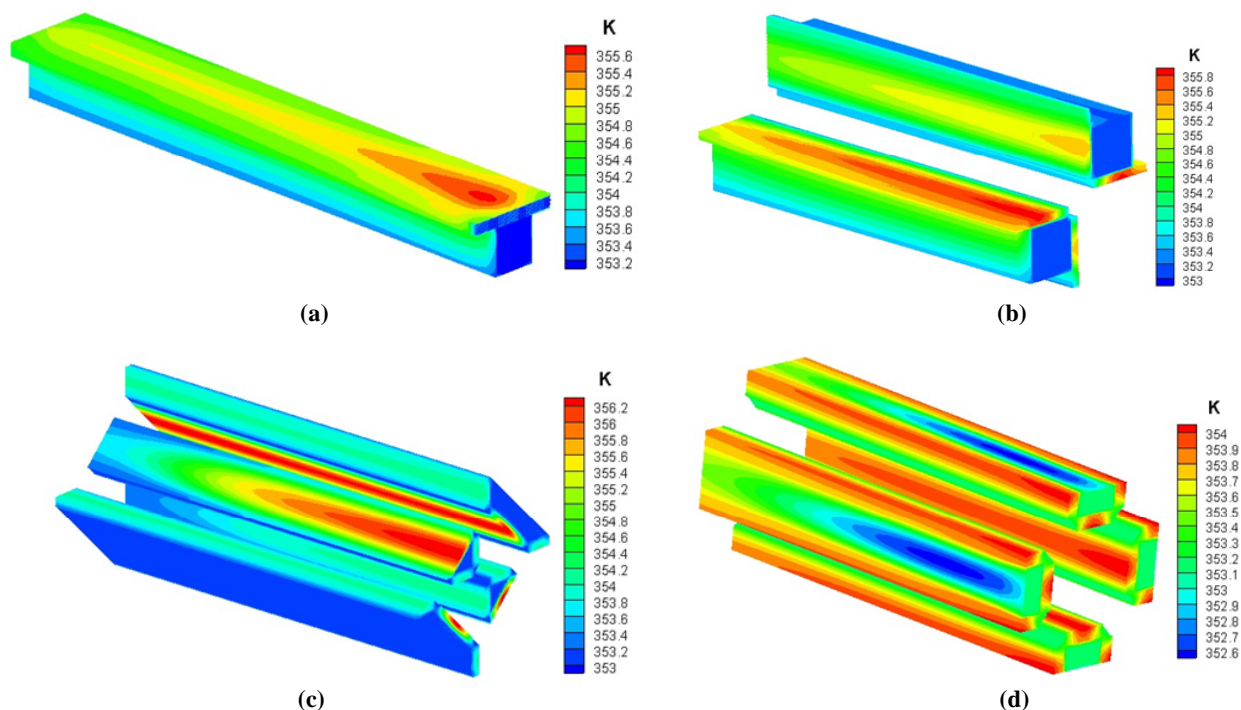


Fig. 7. The distribution of temperature along the cathode electrode of the cell for a) case one, b) case two, c) case three, and d) case four at the 0.4 V of cell potential.

channels helps to achieve enhanced quantity and uniformity in current density due to the fact that separated channels as well as the mentioned plates play the role of electrons transfer and collectors for the external circuit. So, the second and third configuration indicates better performance due to the dispersion and multiplicity of plates and channels.

The electrical connections between anode and cathode bipolar plates, named the external circuit, is significant for completion of the electro-chemical reaction's chain. Each mono-cell in the fourth case, as the best output efficiency provider, includes sixteen bipolar current collectors, (eight for anode and eight for cathode electrodes). By connecting the contact surfaces of the bipolar plates to each other, an anode/cathode terminal of the external circuit will be formed (as shown in the Fig. 9) to transfer electrons from the anode to cathode terminal. Results of the electrical analysis, as shown by the transfer current at the anode/cathode catalyst layers in Fig. 10, show that the maximum magnitude occurs at the anode catalyst layers where the electrons are produced during the electro-chemical reaction.

The advantage of this design is that the bipolar

plates stay at the nearest distance to the catalyst layers which aids in a more efficient collection of electrical charges. Furthermore, the multiplicity of bipolar plates provide a comprehensive network for electron collecting instead of decreasing the potential losses. Fig. 11 indicates the current flux density magnitude at the mono-cell. As is obvious, the anode and cathode external contact surfaces of the bipolar plates present maximum flow through the external electrical circuit.

6. Conclusion

In this research, PEM fuel cell performance enhancement by increasing the multiplicity of cathode channels connected with an anode channel was investigated numerically. To assess the level of enhancement, four cases with the connections of each anode flow channel to one, two, three and four cathode reactants flow fields were considered and the enhancements were compared. The highlights of the present study are listed below:

(I) The exposure of reactants to the membrane

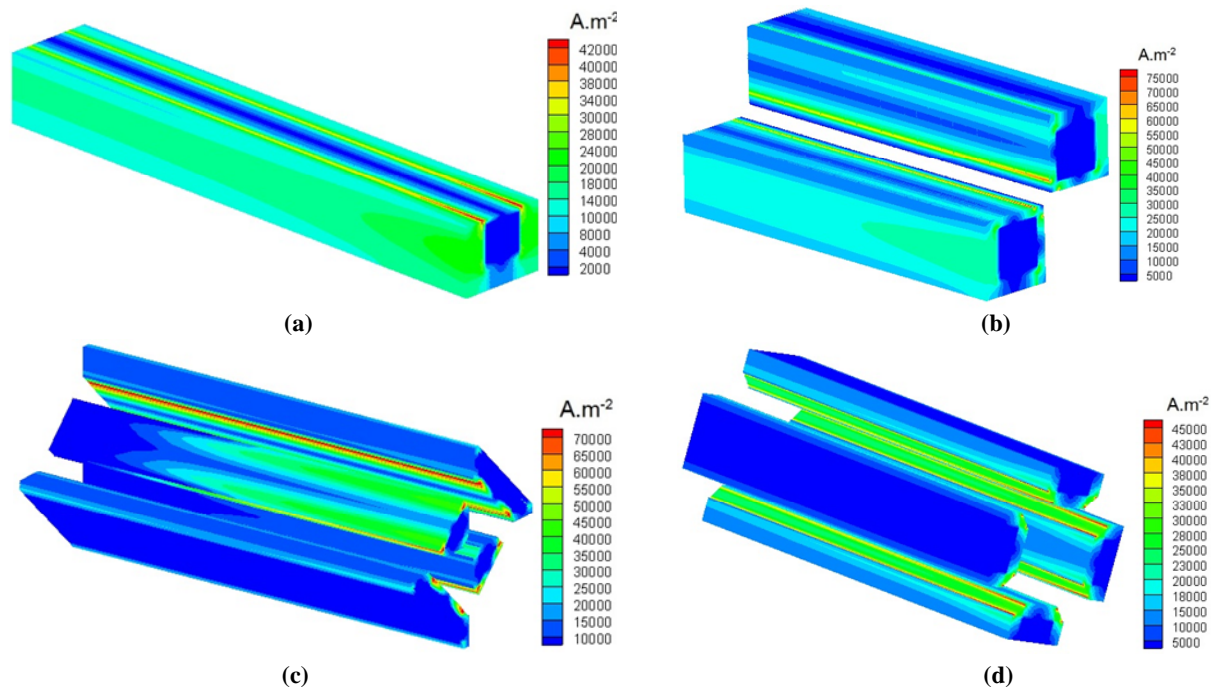


Fig. 8. The distribution of current density along cathode electrode of the cell for a) case one, b) case two, c) case three, and d) case four at the 0.4 V of cell potential.

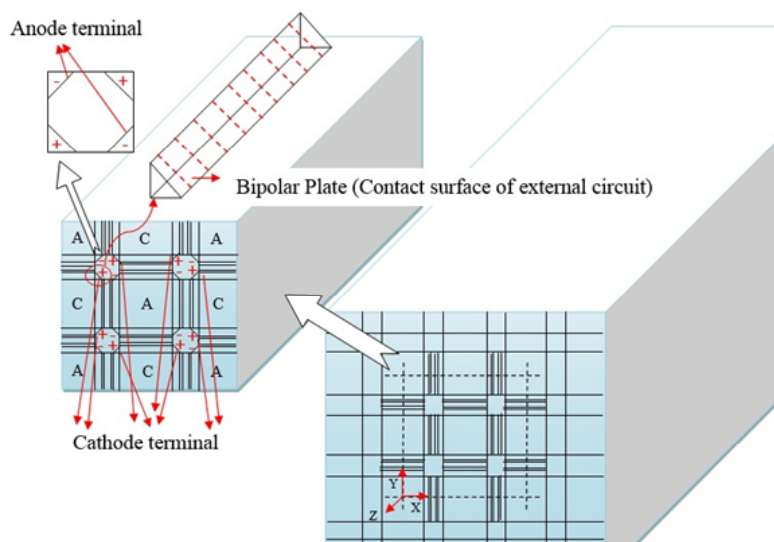


Fig. 9. The anode/cathode external contact surfaces of the bipolar plates (Case Four).

electrode assembly was increased per unit volume.
 (II) The uniformity of reactants mass fraction, temperature and current density distributions were improved.
 (III) Sensible enhancement of power and current densities were achieved (The highest value occurred in the fourth case) with a constant reaction active area and efficient bipolar plates.

(IV) Considerable performance enhancement along with the sensible reduction of cell volume size as well as the mono-cell costs for the new cases in comparison with the base design (~25%) was achieved. The proposed cases were superior to the base model PEM fuel cell from the stand point of performance, cell size and commercial cost. Specifically, the third and fourth cases can generate considerable higher

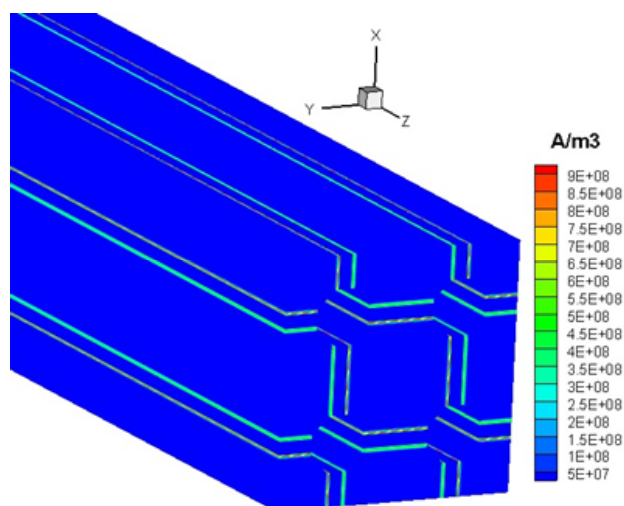


Fig. 10. The distribution of transfer current (A/m^3) at the anode/cathode catalyst layers (Case Four).

power density due to a high rate of output current densities at the optimum volume.

Nomenclature

a	Water activity
A	Area (m^2)
C	Molar concentration (mol/m^3)
D	Mass diffusion coefficient (m^2/s)
E	Electrode potential (V)
E_{eq}	Equilibrium potential (V)
F	Faraday constant (C/mol)
I	Local current density (A/m^2)
i_0	Exchange current density (A/m^2)
k	Thermal conductivity (W/K.m)
K	Permeability (m^2)
M	Molecular weight (kg/mol)
nd	Electro-osmotic drag coefficient
P	Pressure (Pa)
R	Universal gas constant (J/mol.K)
S	Entropy (J/K)
T	Temperature (K)
t	Thickness (m)
u	Vector of velocity (m/s)
V	Cell voltage (V)
V_{oc}	Open-circuit voltage (V)

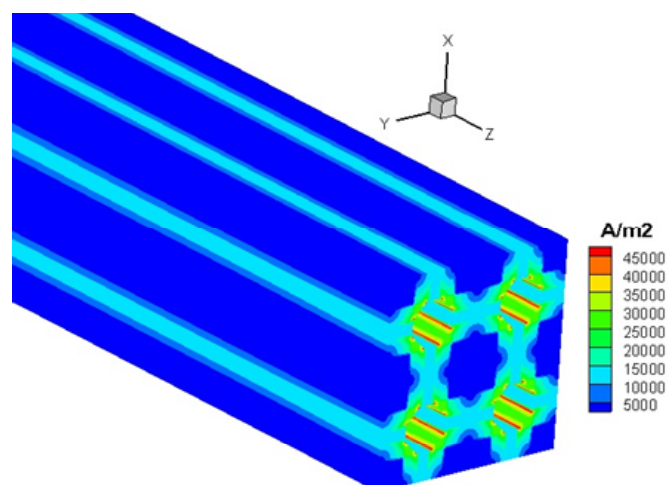


Fig.11. The distribution of current flux density magnitude (A/m^2), (Case Four).

W	Width (m)
X	Mole fraction
Y	Mass fraction
z	Number of electrons involved in electrode reaction

Greek Letters

α	Charge transfer coefficient, (dimensionless)
μ	Viscosity (kg/m.s)
ζ	Stoichiometric ratio
λ	Water content of membrane
σ_e	Membrane ionic conductivity (1/ohm.m)
ε	Porosity
η	Over potential (V)
ρ	Density (kg/m^3)
φ	Potential (V)

Subscripts and Superscripts

a	Anode
avg	average
c	Cathode
ch	Channel
cl	Catalyst
eff	Effective

GDI	Gas diffusion layer
k	Chemical species
m	Membrane
MEA	Membrane electrolyte assembly
ref	Reference value
sat	Saturated
w	water

References

- [1] Xing L., Cai C., Liu X., Liu C., Scott K., Yan Y., "Anode partial flooding modeling of proton exchange membrane fuel cells: Optimization of electrode properties and channel geometries", *Chemical Engineering Science*, 2016, 146:88.
- [2] Jeon Y., Na H., Hwang H., Park J., Hwang H., Shul Y., "Accelerated life-time test protocols for polymer electrolyte membrane fuel cells operated at high temperature", *Int J Hydrogen Energy*, 2015, 40:3057.
- [3] Verma A., Pitchumani R., "Influence of transient operating parameters on the mechanical behavior of fuel cells", *Int J Hydrogen Energy*, 2015, 40:8442.
- [4] Taspinara R., Litster S., Kumbur EC., "A computational study to investigate the effects of the bipolar plate and gas diffusion layer interface in polymer electrolyte fuel cells", *Int J Hydrogen Energy*, 2015, 40:7124.
- [5] Kim YS., Kim SI., Lee NW., Kim MS., "Study on a purge method using pressure reduction for effective water removal in polymer electrolyte membrane fuel cells", *Int J Hydrogen Energy*, 2015, 40:9473.
- [6] Sadeghifar H., Djilali N., Bahrami M., "Thermal conductivity of a graphite bipolar plate (BPP) and its thermal contact resistance with fuel cell gas diffusion layers: effect of compression, PTFE, micro porous layer (MPL), BPP out-of-flatness and cyclic load", *J Power Sources*, 2015, 273:96.
- [7] Sadeghifar H., Djilali N., Bahrami M., "A new model for thermal contact resistance between fuel cell gas diffusion layers and bipolar plates", *J Power Sources*, 2014, 266:51.
- [8] Sadeghifar H., Djilali N., Bahrami M., "Effect of polytetrafluoroethylene (PTFE) and micro porous layer (MPL) on thermal conductivity of fuel cell gas diffusion layers: modeling and experiments", *J Power Sources*, 2014, 248:632.
- [9] Sadeghifar H., Bahrami M., Djilali N., "A statistically based thermal conductivity model for PEMFC gas diffusion layers", *J Power Sources*, 2013, 233:369.
- [10] Wei Zh., Su K., Sui Sh., He A., Du Sh., "High performance polymer electrolyte membrane fuel cells (PEMFCs) with gradient Pt nanowire cathodes prepared by decal transfer method", *Int J Hydrogen Energy*, 2015, 40:3068.
- [11] Mert SO., Ozcelik Z., Dincer I., "Comparative assessment and optimization of fuel cell", *Int J Hydrogen Energy*, 2015, 40:7835.
- [12] Limjeearajarus N., Charoen-amornkitt P., "Effect of different flow field designs and number of channels on performance of a small PEFC", *Int J Hydrogen Energy*, 2015, 40:7144.
- [13] Arvay A., French J., Wang JC., Peng XH., Kannan AM., "Nature inspired flow field designs for proton exchange membrane fuel cell", *Int J Hydrogen Energy*, 2013, 38:3717.
- [14] McKahn DA., "Influence of gas channel depth in self humidified miniature PEM fuel cells with dead-ended anode", *Int J Hydrogen Energy*, 2015, 40:7168.
- [15] Ghanbarian A., Kermani M.J., "Enhancement of PEM fuel cell performance by flow channel indentation", *Energy Conversion and Management*, 2016, 110:356.
- [16] Rahimi-Esbo M., Ranjbar A.A., Ramiar A., Alizadeh E., Aghae M., "Improving PEM fuel cell performance

and effective water removal by using a novel gas flow field:, *Int J Hydrogen Energy*, 2016, 41:3023.

[17] Vazifeshenas Y., Sedighi K., Shakeri S., "Numerical investigation of a novel compound flowfield for PEMFC performance improvement:, *Int J Hydrogen Energy*, 2015, 40:15032.

[18] Torkavannejad A., Sadeghifar H., Pourmahmoud N., Ramin F., "Novel architectures of polymer electrolyte membrane fuel cells: Efficiency enhancement and cost reduction", *Int J Hydrogen Energy*, 2015, 40:12466.

[19] Rostami L., GholyNejad P., Vatani A., "A numerical investigation of serpentine flow channel with different bend sizes in polymer electrolyte membrane fuel cells", *Energy*, 2016, 97 400.

[20] Pourmahmoud N., Rezazadeh S., Mirzaee I., MotalebFaed S., "A computational study of a three-dimensional proton exchange membrane fuel cell (PEMFC) with conventional and deflected membrane electrode", *J Mech Sci Techno*, 2012, 26:2959.

[21] Torkavannejad A., Pourmahmood N., Mirzaee I., Ramin F., "Effect of gas flow channel on the performance of proton exchange membrane fuel cell", *Indian Journal of Science and Technology*, 2014, 4:619.

[22] Imanmehr S., Pourmahmoud N., "Parametric study of bipolar plate structural parameters on the performance of proton exchange membrane fuel cell:, *ASME J Fuel Cell SciTechnol*, 2012, 9:1.

[23] Bilgili M., Bosomoiu M., Tsotridis G., "Gas flow field with obstacles for PEM fuel cells at different operating conditions", *Int J Hydrogen Energy*, 2015, 40: 2303.

[24] Ramin F., Torkavannejad A., Baheri S., "The effect of inclined radial flow in proton exchange membrane fuel cells performance", "Hydrogen of Journal & Cell Fuel, 2014, 3:141.

[25] Tiss F., Chouikh R., Guizani A., "A numerical

investigation of reactants transport in a PEM fuel cell with partially blocked gas channel", *Energy Conversion Management*, 2014, 80:32.

[26] Khazae I., Ghazikhani M., "Three-dimensional modeling and development of the new geometry PEM fuel cell", *Arabian Journal for Science and Engineering*, 2013, 38:1551.

[27] Al-Baghdadi S., Al-JanabiHaroun S., "Parametric and optimization study of a PEM fuel cell performance using three-dimensional computational fluid dynamics model", *Renew Energy*, 2007, 32:107.

[28] Sadeghifar H., Djilali N., Bahrami M., "Thermal conductivity of a graphite bipolar plate (BPP) and its thermal contact resistance with fuel cell gas diffusion layers: effect of compression, PTFE, micro porous layer (MPL), BPP out-of-flatness and cyclic load", *J. Power Sources*, 2015, 273:96.

[29] Marcinkoski J., Jacob S., "Fuel Cell System Cost", *DOE Hydrogen and Fuel Cells Program Record*, September 25, 2014.